INTERNATIONAL JOURNAL FOR NUMERICAL METHODS IN FLUIDS, VOL. 8, 519–536 (1988)

FORCES ON OSCILLATING BODIES IN VISCOUS FLUID

P. G. PATTANI* AND M. D. OLSON

Department of Civil Engineering, University of British Columbia, Vancouver, BC, Canada

SUMMARY

This paper describes a method for determining the fluid forces on oscillating bodies in viscous fluid when the corresponding flow problem has been solved using the finite element method. These forces are characterized by the concept of added mass, added damping and added force. Numerical results are obtained for several example body shapes. Comparison is made with exact analytical results and other finite element results for the limiting cases of Stoke's flow and inviscid flow, and good agreement is obtained. The results for finite values of the body amplitude parameter β show the appearance of added force from the steady streaming component of the flow for asymmetric bodies. Results are also obtained for the associated flow where the fluid remote from a fixed body is oscillating.

KEY WORDS Fluid forces Viscous incompressible flow Fluid–structure interaction Finite element method Steady streaming Added mass Added damping Added force Oscillation flow

INTRODUCTION

Considerable research has been carried out on fluid–structure interaction problems, and today most of the analyses are handled with finite element methods. Most of this work, however, deals with inviscid fluids. A recent symposium[1] covered offshore structural applications. On the other hand, relatively little work has dealt with viscous fluid applications. For example, Belytschko *et al.*[2] and Liu[3] have both considered a general class of problems using a mixed Eulerian–Lagrangian approach. Olson and Pattani[4–6] have developed a method to analyse the periodic flow around an oscillating body with finite amplitude.

This paper describes an extension of this method to determine the fluid forces acting on the oscillating body. For a dynamic system these forces are generally characterized by the concept of added mass, added damping and added force.

It is possible to analyse the case of a body undergoing a harmonic motion in an otherwise still fluid and obtain the flow quantities for the case of a two-dimensional harmonic flow past a similar section by the appropriate transformations. These transformations and the computation of the fluid forces for the associated flow situation are described in this paper.

Numerical results are obtained for three different body shapes, namely, (1) an oscillating circular body, (2) a square body oscillating parallel to one of its sides and (3) a symmetric Joukowski profile oscillating parallel to the line of symmetry. An example flow pattern due to steady streaming for the circular profile is presented and comparison is made with published experimental results. The added mass, added damping and added force are presented for all body shapes. A comparison is

*Now at Department of Aeronautics, University of Texas, Austin, Texas, U.S.A.

0271–2091/88/050519–18$09.00

Received 15 January 1987
Revised 2 June 1987

made with analytical and numerical results for the limiting cases of Stoke's flow and inviscid flow. The following is necessarily brief, but more details are available in Reference 7.

THEORETICAL FORMULATION

The basic theory and finite element formulation which form the basis for the current work are available elsewhere.[4,6] Hence only the essentials needed here are included in the following.

Conservation equations and boundary conditions

The basic equations governing two-dimensional, viscous incompressible fluid flow are the Navier–Stokes equations, the equations of continuity and the boundary and initial conditions. Solution of the flow problem is obtained within a plane domain Ω bounded by a contour Γ which, in general, is composed of two distinct parts, denoted by Γ_u and Γ_s respectively. The well known Navier–Stokes and continuity equations for this problem can be written in the form

$$\begin{aligned}
\frac{Du}{Dt} &= -\frac{1}{\rho}\frac{\partial p}{\partial x} + \nu\left(2\frac{\partial^2 u}{\partial x^2} + \frac{\partial^2 u}{\partial y^2} + \frac{\partial^2 v}{\partial x\,\partial y}\right), \\
\frac{Dv}{Dt} &= -\frac{1}{\rho}\frac{\partial p}{\partial x} + \nu\left(\frac{\partial^2 v}{\partial x^2} + 2\frac{\partial^2 v}{\partial y^2} + \frac{\partial^2 u}{\partial x\,\partial y}\right), \\
\frac{\partial u}{\partial x} &+ \frac{\partial v}{\partial y} = 0,
\end{aligned} \tag{1}$$

where u, v are the x, y components of velocity, ρ, p are the density and pressure respectively, ν is the kinematic viscosity μ/ρ, where μ is the absolute viscosity, and D/Dt is the material derivative.

Boundary conditions are given for velocities on the boundary portion Γ_u, referred to as the kinematic boundary, and tractions over the remaining part Γ_s, the mechanical boundary. That is,

$$\begin{aligned}
&u = \bar{u}, \qquad v = \bar{v} \quad \text{on} \quad \Gamma_u, \\
&\left.\begin{aligned}
\left(-p + 2\mu\frac{\partial u}{\partial x}\right)n_1 + \left[\mu\left(\frac{\partial u}{\partial y} + \frac{\partial v}{\partial x}\right)\right]n_2 &= \bar{X} \\
\left[\mu\left(\frac{\partial u}{\partial y} + \frac{\partial v}{\partial x}\right)\right]n_1 + \left(-p + 2\mu\frac{\partial v}{\partial y}\right)n_2 &= \bar{Y}
\end{aligned}\right\} \quad \text{on } \Gamma_s,
\end{aligned} \tag{2}$$

where $\bar{u}$, $\bar{v}$ are the specified velocities on Γ_u, $\bar{X}$, $\bar{Y}$ are the specified tractions on Γ_s and n_1, n_2 are the direction cosines of the outward-pointing normal to the boundary.

Equation of motion of a rigid body in a fluid

The equation of motion for an elastically supported rigid body of arbitrary shape is given by

$$m\ddot{s} + c\dot{s} + ks = f(t), \tag{3}$$

where m is the mass of the body, c is the structural damping coefficient, k is the elastic spring constant, s is the displacement and the time-dependent loading consists of two components

$$f(t) = F_f(t) + F_e(t), \tag{4}$$

where $F_f(t)$ is the fluid force and $F_e(t)$ is the external force on the body.

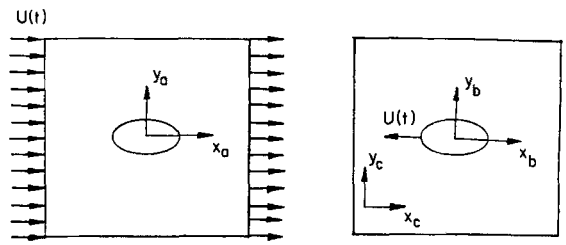

Case I Case II

Figure 1. Comparison of two associated flows

Comparison of two associated flows

We consider an associated pair of two-dimensional flows as defined in Figure 1. In Case I the fluid remote from a stationary body has a uniform time-dependent velocity $U(t)$, and in Case II the identical body has an equal velocity $U(t)$ in the opposite direction, while the fluid remote from the moving body is stationary. These velocities lie in the x direction. The flow quantities in the co-ordinate system fixed to the body in Case I are denoted by subscript a, those fixed relative to the body in Case II by subscript b and those fixed relative to the undisturbed fluid in Case II by subscript c.

Carrying out the transformations between these two cases[7,8,9] leads to the result that

$$u_a = u_b, \qquad v_a = v_b$$

$$\frac{\partial p_a}{\partial y_a} = \frac{\partial p_b}{\partial y_b}, \qquad \frac{\partial p_a}{\partial x_a} = \frac{\partial p_b}{\partial x_b} - \rho \frac{dU}{dt}. \tag{5}$$

The consequence of equation (5) is that the velocities, and hence the 'flow pattern', are identical in both Case I and Case II. The only difference between the two cases as related to pressure is the additional uniform pressure gradient $-\rho\, dU/dt$ in Case I acting in the direction of acceleration.

It is possible to consider the wave flow past a structural member by considering a two-dimensional harmonic flow past a similar section (Sarpkaya and Isaacson[10]). This situation can be obtained by letting $U(t)$ be a harmonic function in Case I. If a problem is analysed in the inertial co-ordinate system (x_c, y_c) as prescribed in Case II for a harmonic velocity $-U(t)$, then it is possible to obtain the flow quantities in the non-inertial co-ordinate system (x_b, y_b). Furthermore, to obtain the flow quantities in Case I for a harmonic $U(t)$ the transformations given by equation (5) can easily be performed. Hence the following analysis is carried out only for Case II.

Non-dimensional form of conservation equations

The problem under consideration is that of a body of arbitrary shape, with a characteristic length b in the direction of motion, undergoing a simple harmonic displacement motion in an otherwise still fluid (Figure 2). The simple harmonic displacement motion of the body is given by

$$s = s_0 \sin(\omega t), \tag{6}$$

where s_0 is the displacement amplitude and ω the impressed frequency. Then the characteristic velocity in the flow is that of the body, namely, $u_0 = \omega s_0$. Introducing the non-dimensional

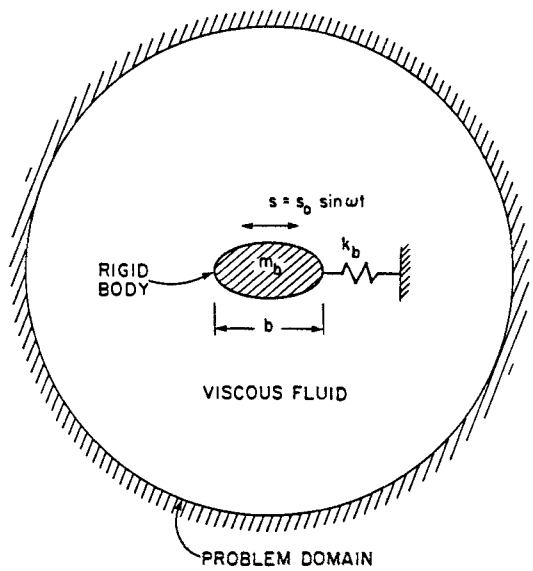

Figure 2. Problem configuration

variables $\tilde{x} = x/b$, $\tilde{y} = y/b$, $\tilde{t} = \omega t$, $\tilde{u} = u/u_0$, $\tilde{v} = v/u_0$, $\tilde{p} = p/\mu u_0/b$ into equation (1) gives

$$\frac{\partial u}{\partial t} + \beta\left(u\frac{\partial u}{\partial x} + v\frac{\partial u}{\partial y}\right) = \frac{1}{R_\omega}\left(2\frac{\partial^2 u}{\partial x^2} + \frac{\partial^2 u}{\partial y^2} + \frac{\partial^2 v}{\partial x\,\partial y} - \frac{\partial p}{\partial x}\right),$$

$$\frac{\partial v}{\partial t} + \beta\left(u\frac{\partial v}{\partial x} + v\frac{\partial v}{\partial y}\right) = \frac{1}{R_\omega}\left(\frac{\partial^2 v}{\partial x^2} + 2\frac{\partial^2 v}{\partial y^2} + \frac{\partial^2 u}{\partial x\,\partial y} - \frac{\partial p}{\partial y}\right), \tag{7}$$

$$\frac{\partial u}{\partial x} + \frac{\partial v}{\partial y} = 0,$$

where all quantities are their respective non-dimensional values and the over tilde has been dropped for convenience. There are two natural Reynolds numbers in the problem, namely, the usual Reynolds number and the frequency Reynolds number given respectively by $Re = u_0 b/\nu$ and $R_\omega = \omega b^2/\nu$. Note that $\beta = Re/R_\omega = s_0/b$ is the body amplitude ratio and is related to the Strouhal number $S = b\omega/u_0$ by $\beta = 1/S$. The corresponding non-dimensional fluid stresses are

$$\sigma_x = -p + 2\frac{\partial u}{\partial x}, \qquad \sigma_y = -p + 2\frac{\partial v}{\partial y}, \qquad \tau_{xy} = \frac{\partial v}{\partial x} + \frac{\partial u}{\partial y} \tag{8}$$

and the non-dimensional form of equation (3) is

$$m\ddot{s} + c\dot{s} + ks = J_b(F_e + F_f), \tag{9}$$

where all stresses have been normalized by $\mu u_0/b$, the forces by $\mu u_0 l$, the mass by $\rho A_b l$ (where A_b is the cross-sectional area of the body and l its length), the damping coefficient by $\omega\rho A_b l$, the stiffness by $\omega^2 \rho A_b l$ and

$$J_b = \frac{\nu u_0}{\omega^2 b A_b} = \frac{\beta}{R_\omega}\frac{b^2}{A_b}. \tag{10}$$

Finite element formulation and solution of equations

Curved isoparametric elements with quadratic interpolation for velocities and bilinear interpolation for the pressure are used to discretize equation (6) as follows:

$$\begin{aligned} u &= N_i u_i(t), \quad i = 1, 2, \ldots, 8, \\ v &= N_i v_i(t), \quad i = 1, 2, \ldots, 8, \\ p &= M_i p_i(t), \quad i = 1, \ldots, 4, \end{aligned} \tag{11}$$

where u_i, v_i, p_i are time-dependent nodal variables and N_i, M_i are shape functions.

These equations are substituted into equation (7) and the Galerkin method is applied to give the elemental equations. When the global equations for a complete problem are assembled from these elemental equations, the moving body boundary conditions are satisfied to order β by a Taylor expansion. This leads to a set of ordinary differential equations of first order in time for the nodal vector **d** made up of velocity components and pressure.

An approximate steady state solution of these equations is obtained by the method of averaging, assuming the solution for **d** for small β is of the form

$$\mathbf{d} = \mathbf{A} + \mathbf{B}(t)\cos t + \mathbf{C}(t)\sin t, \tag{12}$$

where $\mathbf{B}(t)$, $\mathbf{C}(t)$ are assumed to be slowly varying functions of non-dimensional time t. The first term **A** represents the steady streaming[11] part of the solution, which arises naturally for a system with quadratic non-linearities as is encountered here. The averaging technique results in a set of non-linear algebraic equations for the average values of **A**, **B**, **C**. These equations are then solved using a Newton–Raphson procedure.

Determination of fluid forces

Knowing the stress components $\sigma_x, \sigma_y, \tau_{xy}$ at any point P in the two-dimensional fluid domain, the stress on any plane BC through this point and inclined at an angle θ to the x axis can be calculated from

$$\begin{Bmatrix} \sigma \\ \tau \end{Bmatrix} = \begin{bmatrix} \sin^2\theta & \cos^2\theta & -2\sin\theta\cos\theta \\ \sin\theta\cos\theta & -\sin\theta\cos\theta & \sin^2\theta - \cos^2\theta \end{bmatrix} \begin{Bmatrix} \sigma_x \\ \sigma_y \\ \tau_{xy} \end{Bmatrix}, \tag{13}$$

where σ and τ are the normal and shear components respectively of stresses on the plane BC as shown in Figure 3.

For an isoparametric element the co-ordinates of a point in the element are also given by $x = N_i x_i$, $y = N_i y_i$, where the N_i are the shape functions from equation (10) and x_i, y_i are the

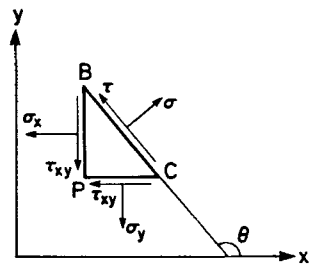

Figure 3. Stress components

nodal co-ordinates. Using equations (11) and the chain rule, the derivatives of the shape functions are given by

$$\begin{Bmatrix} \dfrac{\partial N_i}{\partial s} \\ \dfrac{\partial N_i}{\partial t} \end{Bmatrix} = \begin{bmatrix} \dfrac{\partial N_j}{\partial s} x_j & \dfrac{\partial N_j}{\partial s} y_j \\ \dfrac{\partial N_j}{\partial t} x_j & \dfrac{\partial N_j}{\partial t} y_j \end{bmatrix} \begin{Bmatrix} \dfrac{\partial N_i}{\partial x} \\ \dfrac{\partial N_i}{\partial y} \end{Bmatrix} = [\mathbf{J}] \begin{Bmatrix} \dfrac{\partial N_i}{\partial x} \\ \dfrac{\partial N_i}{\partial y} \end{Bmatrix}, \tag{14}$$

where the matrix **J** is the Jacobian of the transformation. Equations (11) are substituted into equation (8) to obtain

$$\begin{Bmatrix} \sigma_x \\ \sigma_y \\ \tau_{xy} \end{Bmatrix} = \begin{bmatrix} 2\dfrac{\partial N_i}{\partial x} & 0 & -M_i \\ 0 & 2\dfrac{\partial N_i}{\partial y} & -M_i \\ \dfrac{\partial N_i}{\partial y} & \dfrac{\partial N_i}{\partial x} & 0 \end{bmatrix} \begin{Bmatrix} u_i \\ v_i \\ p_i \end{Bmatrix}, \tag{15}$$

where the shape function derivatives are obtained from a numerical inversion of equation (14).

Therefore, to obtain the normal and shear components of the stresses acting on plane BC at point P in the fluid domain, first the derivatives of the shape functions are evaluated using equation (14), then the stress components σ_x, σ_y, τ_{xy} are evaluated using equation (15) and substituted into equation (13).

For a body of general cross-section, the resultant non-dimensional fluid force in the x direction acting on it is given by

$$F_f = -\int (\sigma \sin\theta + \tau \cos\theta)\, dS, \tag{16}$$

where S is the non-dimensional co-ordinate along the boundary and θ is the angle which S makes with the positive x axis.

In general the resultant fluid force F_f on a body oscillating with velocity $u_0 \cos \omega t$ will consist of three components, namely, (1) a component in phase with the acceleration of the body, (2) a component in phase with the velocity of the body and (3) a component which is constant. Therefore the fluid force F_f obtained from equation (16) after integration will be of the form

$$F_f = P + Q \cos t + R \sin t. \tag{17}$$

Computation of added mass, added damping and added force

The non-dimensional displacement of the body, $s = \beta \sin t$, and the fluid force F_f from equation (17) are substituted into equation (9) to obtain

$$F_e = \left(\frac{-m\beta}{J_b} - R\right)\sin t + \left(\frac{c\beta}{J_b} - Q\right)\cos t + \frac{k\beta}{J_b}\sin t - P. \tag{18}$$

The equation of motion can also be written in the form

$$(m + m_a)\ddot{s} + (c + c_a)\dot{s} + ks + f_a = J_b F_e, \tag{19}$$

where m_a, c_a and f_a are the non-dimensional values of the added mass, added damping and added

force respectively. The non-dimensional displacement of the body, $s = \beta \sin t$ is substituted to obtain

$$F_e = \left(\frac{-m\beta}{J_b} - \frac{m_a\beta}{J_b}\right)\sin t + \left(\frac{c\beta}{J_b} + \frac{c_a\beta}{J_b}\right)\cos t + \frac{k\beta}{J_b}\sin t + \frac{f_a}{J_b}. \tag{20}$$

Comparing equation (18) and equation (20), we obtain

$$m_a = \frac{RJ_b}{\beta}, \qquad c_a = -\frac{QJ_b}{\beta}, \qquad f_a = -PJ_b. \tag{21}$$

Therefore, to calculate values of the added mass, added damping and added force, we first carry out the numerical integration as indicated in the previous Subsection to obtain P, Q and R and then use equation (21). Note that the added force is zero for a body which has an axis of symmetry perpendicular to the direction of motion.

NUMERICAL RESULTS

Oscillating circular body

Numerical results are obtained for a circular body with diameter b of unit value with its centroid located at the origin of the x–y co-ordinate system. The body is performing oscillations parallel to the x axis. The computations were performed for a grid corresponding to $D_o/b = 30$, where D_o is the diameter of the outer fixed cylinder.[6] This particular geometry was chosen to correspond to the experimental results of Tatsuno.[12] Detailed comparisons are shown in Reference 6 and only an illustrative example is shown here for the convenience of the reader.

The experimental results in the form of steady streamlines (for the streaming flow) are shown in Figure 4 for $R_\omega = 278{\cdot}2$ and $\beta = 0{\cdot}046$, whereas the numerical results are shown for the same value of R_ω and two values of β, namely, 0·038 and 0·043. The numerical result for $\beta = 0{\cdot}046$ did not converge even when the solution for $\beta = 0{\cdot}043$ was used as an initial guess solution. As explained in Reference 6, this may represent a bifurcation point close to $\beta = 0{\cdot}046$ for transition to a different flow pattern.

Both the numerical and the experimental results clearly show the appearance of the secondary vortices close to the body. There is very good agreement between the experimental and numerical results regarding the flow pattern and the location of both the vortices in each quadrant. However, the numerical results slightly underpredict the thickness of the secondary vortices.

Several approximate analytical solutions of this problem have been published, the most recent and apparently most accurate being that by Wang.[13] However, his solution is restricted to small Reynolds numbers R such that $RS \gg 1$ and $R/S \ll 1$, where S is the Strouhal number based on the radius. In the present notation, $R = Re/2$ and $S = 1/2\beta$. Hence for the experimental result shown in Figure 4 ($R_\omega = 278{\cdot}2$, $\beta = 0{\cdot}046$, $Re = 12{\cdot}8$) $RS = R_\omega/4 = 69{\cdot}6$ and $R/S = \beta^2 R_\omega = 0{\cdot}59$. This would appear to preclude using Wang's result for this case. Furthermore, according to Figure 3 in Wang's paper[13] (which apparently has its abscissa mislabelled S/R rather than RS), for a value of $RS = 69{\cdot}6$ the thickness of the secondary vortices should be over 80% of the radius. (Actually the curve is very steep here and clearly unreliable.) This prediction is obviously contradicted by Tatsuno's experiment and the present numerical results, which show this size to be about 30%.

Added mass and added damping quantities are presented for a range of β and R_ω values including the linear case of $\beta = 0$. Stuart[14] has presented analytical results for this case. Therefore a direct comparison is possible and the results are presented graphically in Figures 5 and 6. The agreement between the exact analytical results and the finite element results is very good.

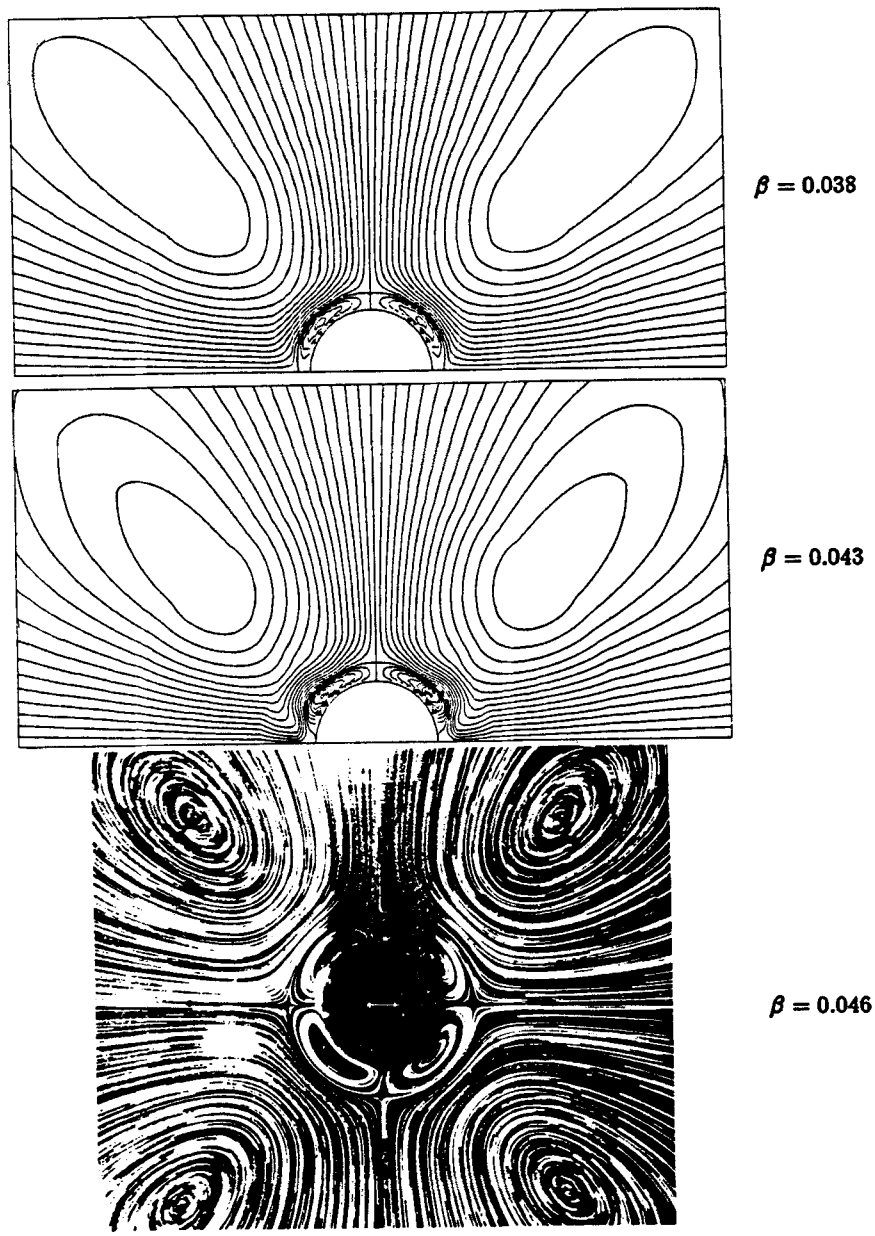

Figure 4. Steady streamlines for oscillating circular body for $R_\omega = 278{\cdot}2$, $D_o/b = 30$

The comparison is also made with the limiting case of inviscid flow. The added mass and added damping values for a bluff body oscillating at high frequency with a small amplitude are not affected much by viscosity. Hence the values of m_a and c_a for large values of R_ω and $\beta = 0$ should approach the values predicted by inviscid flow. The results obtained for this case are presented in Table I. For $R_\omega = 10\,000$ the value of the added mass obtained herein is 1·0607 as compared with 1 for the inviscid flow.[10] The value of the added damping approaches zero as it should.

The results for the added mass and added damping for $\beta = 0, 0{\cdot}03$ and $0{\cdot}1$ are shown graphically

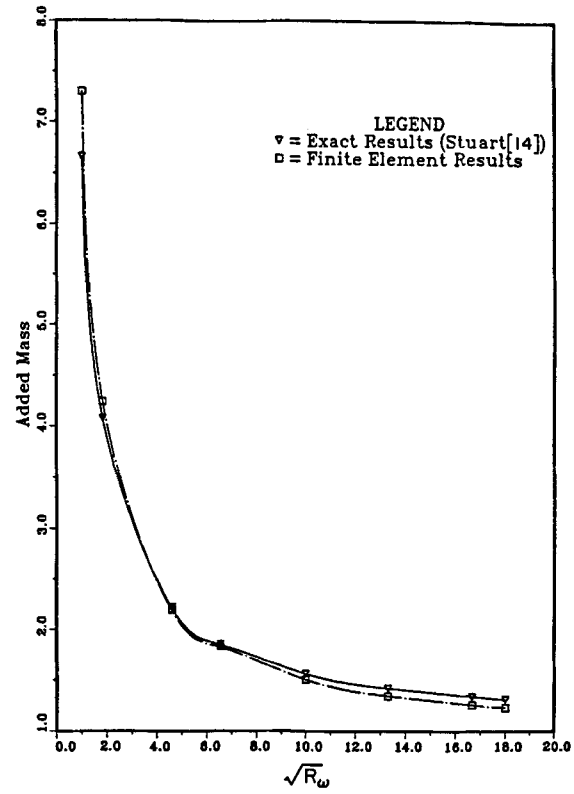

Figure 5. Added mass m_a for oscillating circular body for $\beta = 0$

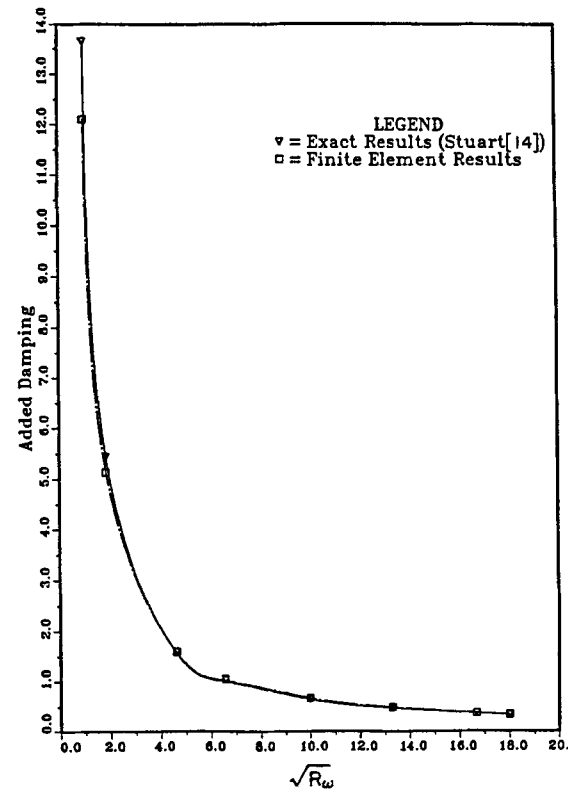

Figure 6. Added damping c_a for oscillating circular body for $\beta = 0$

Table I. Added mass m_a and added damping c_a for oscillating circular body for R_ω large and $\beta = 0$

R_ω	Added mass m_a	Added damping c_a
500	1·177	0·256
5000	1·063	0·039
10000	1·061	0·020
Inviscid[10]	1·0	0·0

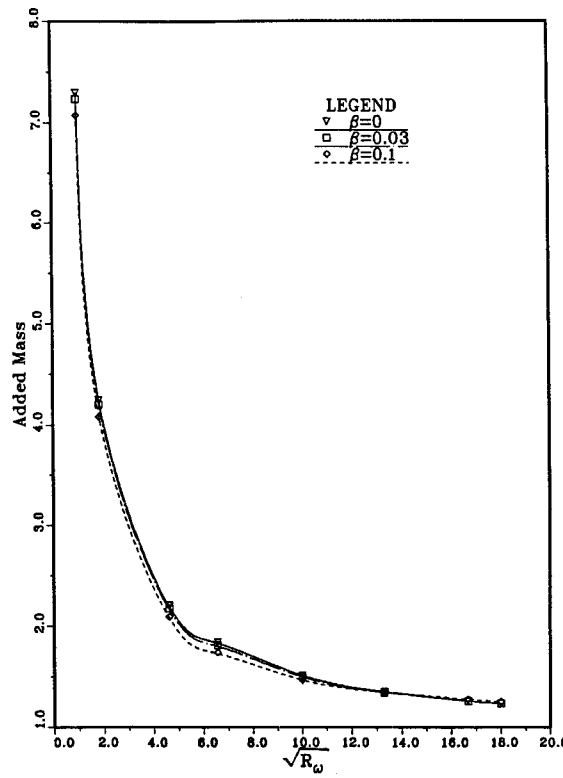

Figure 7. Added mass m_a for oscillating circular body

in Figures 7 and 8 respectively. The result for $\beta = 0{\cdot}03$ shows that the added mass is lower and the added damping is higher than for $\beta = 0$. The same is true for the more complex flow situation of $\beta = 0{\cdot}1$, except at high values of R_ω where the situation is reversed; that is, the added mass terms are higher and the added damping terms lower than for $\beta = 0$. However, in all cases the differences are very small.

Oscillating square body

Numerical results are obtained for a square body of unit size performing harmonic oscillations parallel to one of its sides. Two finite element grids, hereafter referred to as Grid 1 and Grid 2, were used for this problem.[6] Grid 1, a relatively crude grid with $D_0/b = 11$, was used to perform preliminary calculations, while Grid 2 was a more refined grid with $D_0/b = 30$.

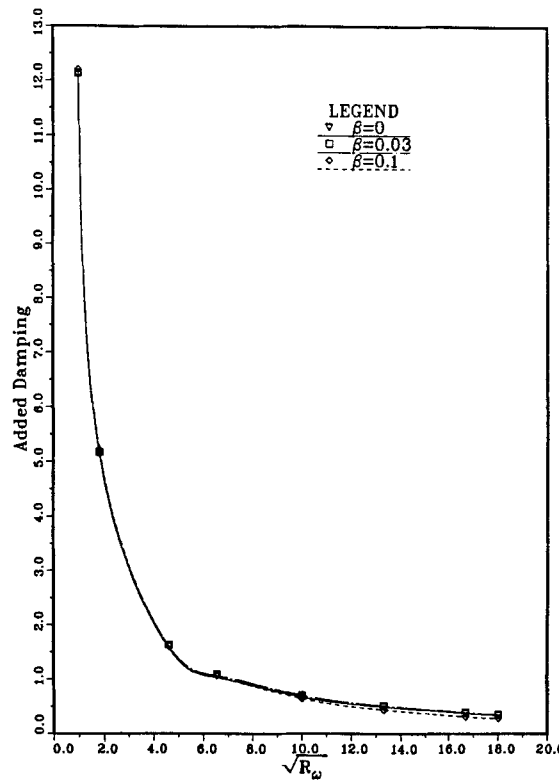

Figure 8. Added damping c_a for oscillating circular body

Table II. Added mass m_a and added damping c_a for oscillating square body for R_ω large and $\beta = 0$

R_ω	Added mass m_a		Added damping c_a	
	Grid 1	Grid 2	Grid 1	Grid 2
500	1·275	1·316	0·061	0·257
5000	1·266	1·238	0·006	0·030
10 000	1·266	1·237	0·003	0·015
Inviscid[9]	1·19		0	

The added mass and added damping quantities are presented for a range of β and R_ω values including the linear case of $\beta = 0$. Owing to the non-availability of any analytical results to make a direct comparison, finite element results for m_a obtained by Irani[15] are used for this purpose. Irani used the streamfunction formulation of the Navier–Stokes equations and the 18 degrees of freedom quintic element for the finite element interpolation of the fluid domain.

The values of the added mass and added damping for large values of R_ω and $\beta = 0$ for both grids are presented in Table II. Theoretically, in the limit of very high frequencies m_a should approach the value predicted for inviscid flow. The limiting value $m_a = 1{\cdot}24$ predicted using Grid 2 and $m_a = 1{\cdot}27$ using Grid 1 are within 4% and 6·5% respectively of the inviscid value of 1·19. The value for the added damping c_a approaches zero for both grids as it should. This indicates that

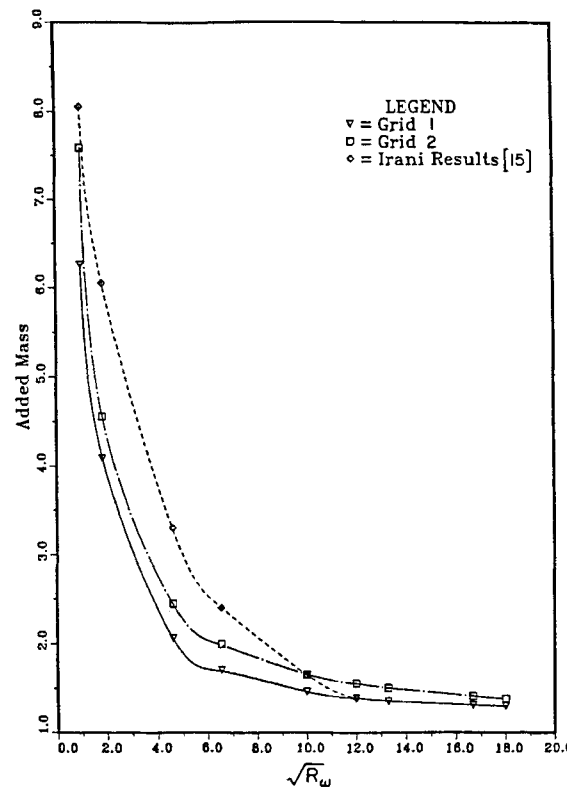

Figure 9. Added mass m_a for oscillating square body for $\beta = 0$

the accuracy and representation of the flow phenomena for the linear case are very good and the results improve with grid refinement as they should.

For moderate values of R_ω the values of the added mass for the linear case obtained using both grids and those obtained by Irani[15] are presented graphically in Figure 9. The values of m_a obtained using Grid 1 are consistently lower than those obtained using Grid 2 except in the limiting case of very large R_ω, where the result for Grid 2 is closer to the inviscid value and lower than for Grid 1. The values of m_a obtained using Grid 2 are close to the results obtained by Irani except for the limiting case of very large R_ω, where Irani's result approaches unity rather than 1·19 for the inviscid case.

The added damping results for the linear case are shown in Figure 10 for moderate values of R_ω. The values of c_a obtained using Grid 1 are consistently lower than those obtained using Grid 2 except for $R_\omega = 1$. For the limiting case of large R_ω the results from both grids approach zero as they should.

The numerical results for added mass and added damping for finite values of β are presented in Table III. For this case there are no published results for comparison. The results in Table III show a general trend of decreasing m_a and c_a with increasing R_ω, similar to the linear case. Also, it is observed that the values of m_a and c_a show only a small change with the small change in β and values are close to the values for the linear case for the β values considered here.

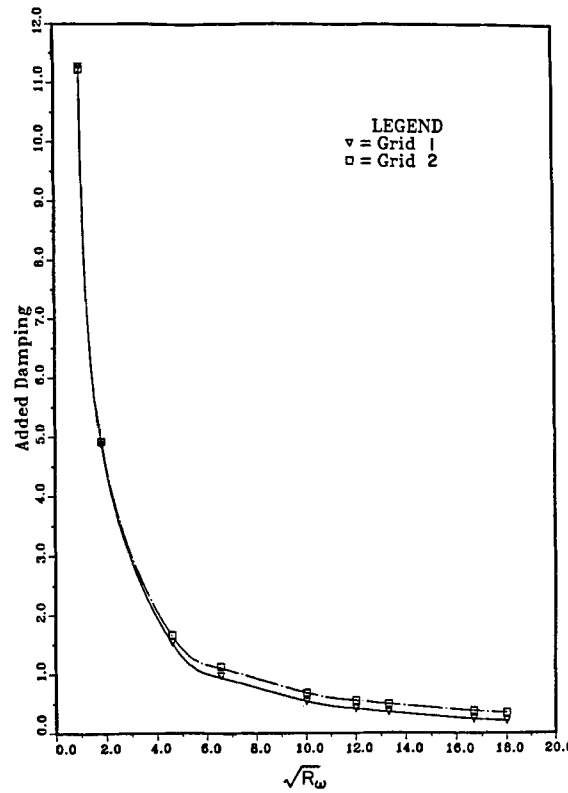

Figure 10. Added damping c_a for oscillating square body for $\beta = 0$

Table III. Added mass m_a and added damping c_a for oscillating square body

R_ω	β	Added mass m_a	Added damping c_a
1·99	0·06	5·40	7·20
1·99	0·1	5·62	6·78
26.01	0·06	2·19	1·71
26·01	0·1	2·30	1·23
120	0·08	1·67	0·28
120	0·1	1·64	0·41
566·44	0·0376	1·31	0·23
566·44	0·058	1·31	0·25

Oscillating symmetric Joukowski profile

The symmetric Joukowski profile used for numerical computation is obtained by introducing the conformal transformation

$$z = \frac{3}{4}\left(\zeta - \frac{1}{2} + \frac{1}{4\zeta - 2}\right), \tag{22}$$

which transforms the region outside the Joukowski profile in the z plane onto the region outside

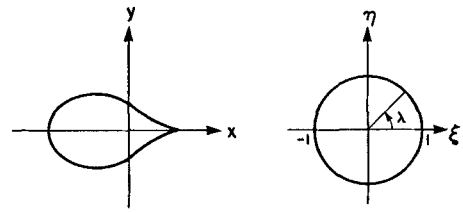

Figure 11. Physical z plane and ζ plane

Table IV. Added mass m_a and added damping c_a for oscillating Joukowski profile for R_ω large and $\beta = 0$

R_ω	Added mass m_a	Added damping c_a
500	0·899	0·397
5000	0·695	0·079
10000	0·683	0·043
1×10^6	0·678	0·003
Inviscid (Appendix)	0·687	0

the unit circle in the ζ plane (see Figure 11). The chord length is chosen as the characteristic length b with unit value. Numerical results are obtained for the body performing oscillations parallel to the x axis using the grid corresponding to $D_0/b = 18{\cdot}3$ in Reference 6.

The added mass, added damping and added force quantities are presented for a range of R_ω and β values including the linear case of $\beta = 0$. The oscillating symmetric Joukowski profile exhibits a finite added force as a result of its asymmetry in the x direction but only for finite β.

The values of m_a and c_a for large values of R_ω and the linear case of $\beta = 0$ are presented in Table IV. As R_ω increases, the value of added mass seems to converge rapidly to a value slightly lower than the theoretical value given in the Appendix but only by 1·5%. The value of c_a approaches zero as it should.

The values of the added mass and added damping for moderate values of R_ω and $\beta = 0$ are shown graphically in Figures 12 and 13 and the corresponding values for finite β are tabulated in Table V.

The results in Table V show a general trend of decreasing values of m_a and c_a with increasing R_ω, the same as for the linear case shown in Figures 12 and 13. It is also observed that m_a and c_a change very little with β for the values of β considered here. Generally, the added force increases with increasing R_ω except for one case; that is, for $R_\omega = 206$ and $\beta = 0{\cdot}0325$ the added force is negative (but small), which apparently is associated with an abrupt change in flow pattern.[6]

Results for associated flow

In the foregoing the results have been presented for the case of a body oscillating with velocity $U(t) = u_0 \cos(\omega t)$ in an otherwise undisturbed fluid. As discussed earlier, it is fairly easy to obtain the corresponding results for a stationary body in a flow field where the far field has a horizontal velocity $u = -u_0 \cos(\omega t)$, since the only essential difference in the flow fields is the uniform pressure gradient $-\rho\, \partial U/\mathrm{d}t$. Hence it is easy to show[7] that the relation between the velocities and

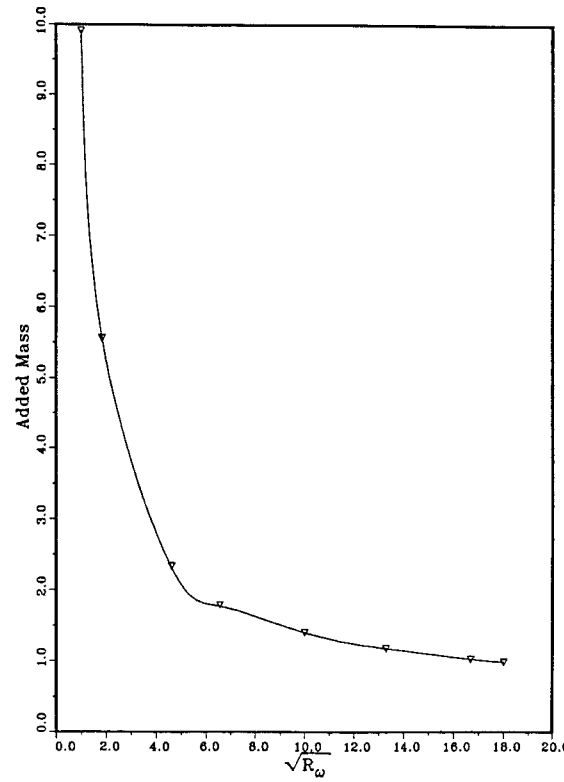

Figure 12. Added mass m_a for oscillating Joukowski profile for $\beta = 0$

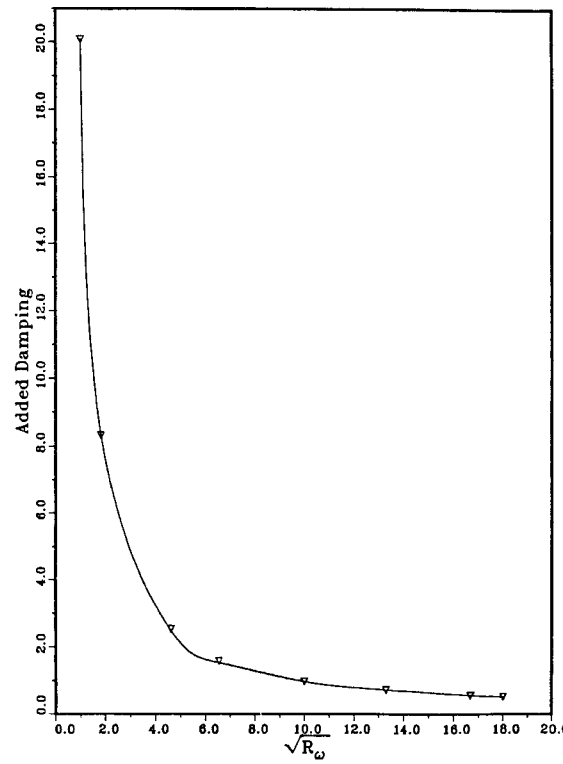

Figure 13. Added damping c_a for oscillating Joukowski profile for $\beta = 0$

Table V. Added mass m_a, added damping c_a and added force f_a for oscillating Joukowski profile

R_ω	β	Added mass m_a	Added damping c_a	Added force f_a
55·1	0·01	1·65	1·36	$0{\cdot}63 \times 10^{-5}$
55·1	0·064	1·56	1·43	$0{\cdot}97 \times 10^{-3}$
55·1	0·1	1·69	1·35	$0{\cdot}32 \times 10^{-2}$
206	0·0091	1·12	0·67	$0{\cdot}30 \times 10^{-5}$
206	0·0131	1·12	0·67	$0{\cdot}59 \times 10^{-5}$
206	0·0188	1·12	0·68	$0{\cdot}11 \times 10^{-4}$
206	0·0251	1·11	0·69	$0{\cdot}16 \times 10^{-4}$
206	0·0325	1·08	0·74	$-0{\cdot}40 \times 10^{-5}$
206	0·0622	1·14	0·60	$0{\cdot}23 \times 10^{-3}$
206	0·1	1·19	0·61	$0{\cdot}10 \times 10^{-2}$

pressure in the two co-ordinate systems shown in Figure 1 is

$$u_a = u_c + \cos t, \qquad v_a = v_c, \qquad p_a = p_c + R_\omega x_a \sin t + K, \tag{23}$$

where K is simply an integration constant; and the corresponding relation between the added mass, added damping and added force is

$$(m_a)_a = (m_a)_c + 1, \qquad (c_a)_a = (c_a)_c, \qquad (f_a)_a = (f_a)_c. \tag{24}$$

Therefore, to evaluate (i) the velocities and pressure and (ii) the added mass, added damping and added force for the case of oscillatory flow remote from the fixed body when the respective results are available for the case of the oscillating body in an otherwise undisturbed fluid, equations (23) and (24) respectively are used.

CONCLUDING REMARKS

The present method of determining the fluid forces on oscillating bodies in viscous fluid seems to work well for the range of parameters studied here. Although the parameter limits of applicability have not been fully explored as yet, there are some obvious limits. Since the oscillating body boundary conditions are expanded only to order β, then β should be kept small, perhaps $\leqslant 0{\cdot}2$. For small β there seems to be no limit on the frequency Reynolds number R_ω. However, there are practical limits on the Reynolds number Re in that, as Re increases, the flow field becomes more complex (the boundary layer becomes thinner) and the finite element grid must be refined.

The results for the added mass and added damping for the linear case of $\beta = 0$ compare very well with other finite element results and exact analytical results. Furthermore, they seem to approach the correct limiting values for the inviscid flow when R_ω is large. New results for the added mass, added damping and added force have been obtained for finite values of the body amplitude parameter β. From these results it is observed that the effect of β on the added mass and added damping is very small (at least up to $\beta \approx 0{\cdot}1$). The steady streaming component of flow does not create any added force on bodies which are oscillating perpendicular to the axis of symmetry (circle and square), but does lead to finite values for asymmetric bodies such as the Joukowski profile.

ACKNOWLEDGEMENTS

This work has been supported by the Canadian Natural Sciences and Engineering Research Council. The helpful comments of one of the reviewers which led to significant improvements in the paper are also gratefully acknowledged.

APPENDIX. INVISCID CALCULATIONS FOR JOUKOWSKI PROFILE

The total potential for a body having translation velocity $U(t)$ in the x direction can be expressed as (see Newman[16])

$$\phi = U\phi_1. \tag{25}$$

The potential defined by (25) satisfies the body boundary condition provided ϕ_1 satisfies the condition

$$\partial\phi_1/\partial n = n_1, \tag{26}$$

where the outward-pointing unit normal vector to the body is given as $\mathbf{n} = n_1\mathbf{i} + n_2\mathbf{j}$. This unit normal vector can be written as

$$\mathbf{n} = \sin\theta\,\mathbf{i} + \cos\theta\,\mathbf{j}, \tag{27}$$

where θ is the angle which the co-ordinate S along the boundary makes with the positive x axis. Therefore the boundary condition (26) can be written as

$$\partial\phi_1/\partial n = \sin\theta. \tag{28}$$

The added mass for such a body is given as

$$m_a = \rho l \int \phi_1 \sin\theta\,\mathrm{d}S, \tag{29}$$

where ρ is the fluid density and l is the axial length of the body. Introducing non-dimensional variables

$$\tilde{m}_a = m_a/\rho l A_b, \qquad \tilde{S} = S/b, \qquad \tilde{\phi}_1 = \phi_1/b$$

into equation (29), we obtain

$$m_a = (b^2/A_b)\int \phi_1 \sin\theta\,\mathrm{d}S, \tag{30}$$

where all quantities are their respective non-dimensional values and the over tilde has been dropped for convenience.

The complex potential F for inviscid flow past the Joukowski profile (see Figure 11) with unit x-velocity at infinity is given in the ζ plane as (see Tamada and Miyagi[17])

$$F = \tfrac{3}{8}(\zeta - 1/\zeta). \tag{31}$$

The complex potential F for the Joukowski profile moving with unit x-velocity in an otherwise undisturbed fluid differs from (31) by the free stream potential provided the relative velocity between the body and the fluid at infinity is the same in both cases (see Newman[16]). Therefore the complex potential for this case is given as

$$F = \tfrac{3}{8}(\zeta + 1/\zeta) - x. \tag{32}$$

To obtain ϕ_1 from (32), we take the real part of F and note the fact that $\zeta = \mathrm{e}^{\mathrm{i}\lambda}$ on the body. This results in

$$\phi_1 = \tfrac{3}{4}\cos\lambda - x. \tag{33}$$

Substituting equation (33) into (30), we obtain

$$m_a = (b^2/A_b) \int \tfrac{3}{4} \cos\lambda \sin\theta \, dS - 1, \tag{34}$$

where the fact that $\int x \sin\theta \, dA = A_b/b^2$ by applying Green's theorem in the plane has been used.

The integration in (34) is evaluated using Gauss quadrature and the co-ordinate transformation given by equation (22). The non-dimensional cross-sectional area of the Joukowski profile under consideration is computed to be $A_b/b^2 = 0{\cdot}3927$ and the corresponding added mass using 10-point Gauss quadrature is computed to be $m_a = 0{\cdot}6874$.

REFERENCES

1. H. Armen and S. Stiansen (eds), *Computational Methods for Offshore Structures (Symposium)*, ASME, AMD Vol. 37, 1980.
2. T. Belytschko, J. M. Kennedy and D. F. Schoeberle, 'Quasi-Eulerian finite element formulation for fluid–structure interaction', *J. Pressure Vessel Technol., Trans. ASME*, **102** (1), 62–69 (1980).
3. W. K. Liu, 'Finite element procedures for fluid–structure interactions and applications to liquid storage tanks', *Nucl. Eng. Des.*, **65** (2), 221–238 (1982).
4. M. D. Olson and P. G. Pattani, 'Nonlinear analysis of rigid body–viscous flow interaction', in R. H. Gallagher *et al.* (eds), *Finite Elements in Fluids*, Vol. 6, Wiley, Chichester 1985, pp. 307–320.
5. P. G. Pattani and M. D. Olson, 'Stability of nonlinear solutions of rigid body–viscous flow interaction', *Proc. 4th Int. Conf. on Numerical Methods in Laminar and Turbulent Flow*, Swansea, 8–13 July 1985, pp. 1182–1193.
6. P. G. Pattani and M. D. Olson, 'Periodic solutions of rigid body–viscous flow interaction', *Int. j. numer. methods fluids*, **7**, 653–696 (1987).
7. P. G. Pattani, 'Nonlinear analysis of rigid body–viscous flow interaction', *Ph.D. Thesis*, Department of Civil Engineering, University of British Columbia, Vancouver, 1986.
8. M. de St. Q. Isaacson, 'The forces on circular cylinders in waves', *Ph.D. Thesis*, University of Cambridge, 1974.
9. G. K. Batchelor, *An Introduction to Fluid Dynamics*, Cambridge University Press, London, 1974, pp. 139–140.
10. T. Sarpkaya and M. Isaacson, *Mechanics of Wave Forces on Offshore Structures*, Van Nostrand Reinhold Company, New York, 1981.
11. H. Schlichting, *Boundary Layer Theory*, 6th Edn, McGraw-Hill 1968.
12. M. Tatsuno, 'Secondary flow around oscillating asymmetric cylinders', *Reports of Research Institute of Applied Mechanics, Kyushu University, Vol. XXVIII, No. 89*, 1980, pp. 35–47.
13. Chang-Yi Wang, 'On high-frequency oscillatory viscous flows', *J. Fluid Mech.*, **32** (Part 1), 55–68 (1968).
14. J. T. Stuart, 'Periodic boundary layers', in L. Rosenhead (ed.), *Fluid Motion Memoirs—Laminar Boundary Layers*, Oxford University Press, Oxford 1963, p. 390.
15. M. B. Irani, 'Finite element analysis of viscous flow and rigid body interaction', *Master's Thesis*, Department of Civil Engineering, University of British Columbia, Vancouver, 1982.
16. J. N. Newman, *Marine Hydrodynamics*, The MIT press, Cambridge, Massachusetts, 1977.
17. K. Tamada and T. Miyagi, 'Secondary flow around an oscillating cylinder', *J. Phys. Soc. Japan*, **37** (1), 249–253 (1974).